Hindawi
Mathematical Problems in Engineering
Volume 2020, Article ID 2515107, 17 pages
https://doi.org/10.1155/2020/2515107

Research Article

Novel Predictive Control for the IPMSM Fed by the 3L-SNPC Inverter for EVAs: Modified Lyapunov Function, Computational Efficiency, and Delay Compensation

Abdiddaim Katkout,[1] **Tamou Nasser**,[2] **and Ahmed Essadki**[1]

[1]*ERERA, Research Center in Sciences and Technologies of Engineering and Health (STIS), ENSET, Mohammed V University, Rabat, Morocco*
[2]*ERERA, Research Center in Sciences and Technologies of Engineering and Health (STIS), ENSIAS, Mohammed V University, Rabat, Morocco*

Correspondence should be addressed to Abdiddaim Katkout; abdiddaim.katkout@um5s.net.ma

Received 13 May 2020; Revised 22 July 2020; Accepted 5 August 2020; Published 27 August 2020

Academic Editor: Laurent Dewasme

Copyright © 2020 Abdiddaim Katkout et al. This is an open access article distributed under the Creative Commons Attribution License, which permits unrestricted use, distribution, and reproduction in any medium, provided the original work is properly cited.

This paper proposes a novel predictive strategy based on a model predictive control (MPC) for the interior permanent magnet synchronous motors (IPMSMs) driven by a three-level simplified neutral-point clamped inverter (3L-SNPC) for electric vehicle applications (EVAs). Based on the prediction of the future behavior of the controlled variables, a predefined multiobjective cost function incorporates the control objectives which are evaluated for every sampling period to generate the optimal switching state applied directly to the inverter without the modulation stage. The control objectives in this paper are tracking current capacity, neutral-point voltage balancing, common-mode voltage control, and switching frequency reduction. The principal concepts of the novel scheme are summarized as follows: first, the delay compensation based on the long horizon of prediction is adopted by a multilevel power converter structure. Second, based on the modified Lyapunov candidate function, both stability and recursive feasibility are ensured of the proposed predictive scheme. Third, the practicability of the real-time implementation is improved by the proposed "static voltage vector" (SVV) and "single state variation" (SSV) principles. Finally, the proposed concepts are implemented in the novel predictive control formulation as additional constraints without compromising the complexity and the good performances of the predictive controller. Therefore, only the switching states that guarantee the stability and the reduction of calculation burden criteria are considered in the evaluation of cost function. The proposed predictive scheme based on the "SVV" principle has demonstrated superior performance in simulation compared with the proposed scheme with the "SSV" principle. The computational burden and switching frequency rates are reduced by 35% and 56.22%, respectively.

1. Introduction

Currently, permanent magnet synchronous machines (PMSMs) are widespread in many electric vehicle applications (EVAs) [1, 2]. Depending on the magnet placement, two categories of the PMSM are defined: surface-mounted PMSM and interior PMSM [3]. Particularly, interior PMSM (IPMSM) demonstrates excellent properties, such as compact structure with small size and weight, higher power density, high torque to inertia ratio, wide speed range operations, low noise, and robustness [4]. Many control strategies for the IPMSM are proposed: linear control with a modulator and nonlinear controls without a modulator [5, 6]. In different aspects, other classifications include robust controllers (RC), adaptive controllers (AC), and intelligent controllers (IC) [7–10].

There are many research studies accorded to ensure a satisfactory control performance of IPMSMs. In [11], the authors propose an online maximum torque per ampere (MTPA) control based on the numerical optimization technique to avoid the large memory usage and the accurate interpolation algorithm required using the look-up table

(LUT) methods. A deadbeat-direct torque and flux control (DB-DTFC) of IPMSM drive for machine parameter variation is presented in [12]. The flux-weakening control strategy for the IPMSM with maximum torque per volt in VAs is presented in [13]. The desired dq-optimal current references are calculated analytically to achieve the operating point regarding the electrical limits. A comparative study on DTC of IPMSM for EVs between DTC combined with space vector modulation (DTC-SVM) and deadbeat DTC (DB-DTC) is presented in [14]. Nevertheless, these existing control strategies are limited by several challenges [15]:

(i) Low dynamic-state performances and need of the internal loop

(ii) Complex modulation stage and sensibility of the system variables

(iii) Controlled variable ripples

To overcome these aforementioned issues, numerous predictive controls (PCs) are proposed to improve the control performances for the power converter applications [16]. Based on the dynamic system model, the PC predicts the future behavior of the controlled system. A predefined cost function incorporates the controlled variables which are minimized every sampling period to generate the optimal switching state $\mu_{abc}^{\text{opt}} = \{\mu_a, \mu_b, \mu_c\}$ [17]. In comparison with the existing control strategies, PC offers many advantages: easy application in a variety of processes and multiple-input-multiple-output (MIMO) systems, system constraints and nonlinearities which can be incorporated directly into the control law, simple controller concept and implementation, and good dynamic and steady-state performances [18]. Furthermore, the computational delay and dead time can be compensated, and several control loops can be incorporated into one control law. The predictive controllers can be divided into two principal categories: Continuous control set MPC and finite control set MPC (FMPC). Particularly, FMPC is the most attractive predictive strategy for power converters [19]. Taking into account the discrete nature of the power converter, FMPC uses the available switching states to formulate the predictive problem algorithm without requiring any table of switches, external modulator stage, or regulator. Little has been published regarding FMPC of IPMSM for EVAs. Linear inequality matrices (LMIs) represent an effective tool to transform the problem of robust PC design into the form of a convex optimization problem [20]. LMIs are a powerful tool to deal with the many optimization problems in control theory, system identification, and signal processing. A robust predictive control with nonsymmetric constraints (NSC) using the LMI framework is presented in [20]. The method is based on three principles: time-varying vector of constraints, switching indicator function to determine the current boundaries, and support controller that certifies the robust stability. Ojaghi et al. [21] proposed an LMI approach to robust predictive control of nonlinear systems (NLS) with state-dependent uncertainties. An LMI approach to mixed-integer predictive control of uncertain hybrid systems with binary and real-valued control inputs is proposed in [22].

Generally, different topologies of power converters are available in the market. The aforementioned control strategies have been mainly limited to a two-level power converter in a variety of IPMSM applications [23–25]. However, the limited switching state combinations available in the two-level power converters (eight possible combinations) lead to high controlled variable ripples as well as voltage and current waveforms with a higher total harmonic distortion. Additionally, this results in higher switching losses and high switching device stress due to the high dv/dt derivative [26].

To address the aforementioned issue and to fulfill the high-performance IPMSM application requirements (e.g., EVAs), numerous multilevel power converter structures are recognized: neutral-point clamped (NPC), flying capacitor (FC), cascade H-bridge (CHB), and modular multilevel (MM) [27–29]. Several researchers have investigated the multilevel power converter, thanks to its benefits: low voltage applied to each component, less dv/dt and low THD of the output voltage and current waveforms, and low switching loss using the redundancy of the switching states [30, 31]. In recent years, the NPC and T-type are the most used multilevel power converter topologies in the industry [32–34]. The system complexity and calculation cost are increasing significantly with the number of switching devices. Maintaining the multilevel output, the 3L-SNPC requires a few switching devices. A comparison in terms of semiconductor device number between 3L-NPC, T-type, and 3L-SNPC is tabulated in Table 1 [35]. Needless to say, the main source of neutral-point voltage fluctuations in NPC and T-type topologies does not exist in the 3L-SNPC topology.

In [33], the authors proposed a predictive control for a grid-tie three-level neutral-point-clamped inverter with dead-time compensation. This predictive control is based on the orientation of grid voltage to predict the performance of control variables required for the system. Using the stability condition through a control Lyapunov function, the execution time is decreased by 26%. In [36], an asymptotically stable mono-objective predictive control of a grid-connected converter based on discrete space vector modulation is proposed. The presented approach combines the concept of discrete space vector modulation (DSVM) into the FMPC structure to improve the input current quality of the power converter. However, the additional virtual voltage vectors can cause an unacceptable computational burden to the controller. To alleviate this issue, the number of possible voltage vectors for the optimization process is reduced by a preselection technique. In this work, we propose to reduce computation burden by the proposed "static voltage vector" (SVV) and "single state variation" (SSV) principles. The computational burden is reduced by 35%. The aspect of reduction of switching frequency is introduced and decreased by 56.22%.

Literally, there is very little research, if any, performed on the predictive control of the multilevel 3L-SNPC inverter. Furthermore, a little has been published regarding the feasibility and stability, delay compensation, and the computational burden reduction of IPMSM driven by a 3L-SNPC inverter.

Table 1: Comparison between multilevel structures.

Semiconductor device	3L-NPC	T-type	3L-SNPC
DC-link capacitor	2	2	2
Active switch	12	12	10
Passive switch	18	12	10
Switch block $U_{DC}/2$	12	6	4
Switch block U_{DC}	0	6	6

Taking into account the EVA requirements, the principal contributions of this paper are summarized as follows:

(i) This paper proposes a novel and promising configuration of EVAs: FMPC predictive control strategy for IPMSM fed by the 3L-SNPC inverter.

(ii) A modified Lyapunov candidate function which guarantees the feasibility and stability by taking into consideration the discrete nature of the power converter is proposed. Both recursive feasibility and stability are embedded in MPC problem formulation as additional constraints.

(iii) Multiobjective predictive problem formulation that includes four control objectives is considered: tracking current capacity, neutral-point voltage balancing, common-mode voltage control, and switching frequency reduction.

(iv) By using a two-step horizon of the prediction approach, the computational delay due to the calculation and communication time is compensated.

(v) In order to guarantee the practicability of the real-time implementation and computational efficiency of the proposed predictive control, "static voltage vector" (SVV) and "single state variation" (SSV) principles are proposed and embedded in MPC problem formulation as additional constraints.

In the novel predictive control in this paper, the aforementioned contributions are explicitly included in the predictive problem formulation without affecting the controller performances and simplicity.

Section 2 presents the preliminaries of principal concepts of this paper. Section 3 describes the system dynamics. The FMPC and proposed predictive control formulation are illustrated in Sections 4 and 5, respectively. In Section 6, detailed simulation verification studies are carried to show the efficiency of the proposed predictive strategies. Finally, Section 7 draws the conclusion. The nomenclature of this paper is summarized in Table 2.

Table 2: Nomenclature.

Superscripts	
r	Reference value
p	Predicted value
m	Measured value
$*$	Delay compensation
opt	Optimal
Subscripts	
ss	Switching states
np	Neutral point
cm	Common mode
i	Current
sw	Switching frequency
Nomenclature	
MPC	Model predictive control
FMPC	Finite control set MPC
I-FMPC	Improved FMPC
MI-FMPC	Modified I-FMPC
CMI-FMPC	Computationally efficient FI-FMPC
SVV	Static voltage vector
Γ	Cost function
Λ	Weighting coefficient
$\mu_{a,b,c}$	Control of the 3L-SNPC inverter
Υ	Lyapunov candidate function (LCF)
Ψ_{dq}	dq-positive gains of (LCF)
SSV	Single state variation

2. Preliminaries

The FMPC is a very attractive solution for controlling power converters and electrical drives. Nonetheless, stability, computational delay, and computational burden reduction are still open issues to be investigated. In this section, a statement about the three aspects is presented.

2.1. Stability. In conventional predictive problem formulation, the stability in the closed loop is not taken into account. It is worth mentioning that the stator reference current i^r cannot be obtained by applying the voltage vectors resulting from the application of available 21 switching states in the 3L-SNPC. Consequently, the equilibrium point is not achieved by some reference values. Accordingly, the optimization loop of the predictive control aims to generate the current value bounded around the reference value, the reason why we focus on practical stability. In this work, the 3L-SNPC multilevel inverter structure is designed to produce the desired output voltage by multiple available switching states instead of limited switching state combinations in two-level inverters [37].

In spite of good dynamic and steady-state performances of the conventional FMPC predictive strategy, the stability, still an open issue, is to be studied. A notable tool to overcome this issue is Lyapunov stability theory [38]. To guarantee stability in the predictive problem formulation, the cost function is considered as Lyapunov candidate function (LCF) between two sampling periods. The stability analysis focuses on showing that such cost function satisfies the conditions of practical LCF [39].

2.2. Impact of Computational Delay. The FMPC algorithm consists of the following steps [40]:

(i) Measurement of controlled variables

(ii) Prediction of future values of controlled variables for the combination of each switching state available in the 3L-SNPC inverter

(iii) Evaluation of predefined cost function for every sampling period

(iv) Selection and application of the optimal switching state that minimizes the cost function

The operating cycle of the FMPC is illustrated in Figure 1. The predicted, reference, and measured values of stator current are presented by dashed black lines, dashed blue lines, and solid black lines, respectively. In the perfect case, due to the negligibility of the calculation time t_c, FMPC algorithm steps are accomplished spontaneously at instance k to generate the optimal switching state $\mu_{abc}^{\text{opt}} = \{\mu_a, \mu_b, \mu_c\}$, Figure 1(a). Consequently, the stator current i^m reaches its reference value i^r at the $k+1$ instance [41]. In the real case, a significant computational delay t_c is required for the operating cycle and communication time, Figure 1(b). The delay between the measurements and the generation of μ_{abc}^{opt} can cause some problems if not considered. Consequently, the previous optimal switching state μ_{abc}^{opt} will continue to be applied during t_c and stator current i^m which will oscillate around its reference i^r, increasing the current undulation. The computational delay affects the system performances and increases the difficulty of its controllability.

To compensate the computational delay, we propose using a long horizon of prediction approach as shown in Figure 1(c). Using the optimal switching state $\mu_{abc}^{\text{opt}}(k)$ and controlled variable values at the k instance, the N_{ss} system state values at the $k+1$ instance are predicted; N_{ss} denotes the switching states available in the inverter. For each predicted value at the $k+1$ instance, N_{ss} future values are predicted at $k+2$. Accordingly, the optimal switching state μ_{abc}^{opt} that minimizes the cost function at the $k+2$ instance is applied directly to the inverter without the modulation stage at the $k+1$ instance [40].

2.3. Computational Efficiency. To compensate the computational delay for the 3L-SNPC inverter, using a two-step horizon of prediction, a discrete set of $21^2 = 441$ possible trajectories of the switching states has to be enumerated for the evaluation of the cost function, Figure 2(a). This proposition led to a large number of computational burden, which makes the real challenge to the actual digital system implementation [42]. To reduce the number of real-time evaluations, this paper proposes a modified two-step horizon prediction using a proposed "static voltage vector" (SVV), Figure 2(b), and "single state variation" (SSV), Figure 2(c), principles.

3. System Dynamics

3.1. IPMSM. A typical dq-coordinate rotating reference frame-based mathematical model in the time domain of IPMSM drive systems is given by [24]

$$u_s^d(t) = Ri_d(t) + L_d\frac{\mathrm{d}i_d}{\mathrm{d}t} - \omega_{\text{erf}}(t)L_q i_q(t), \tag{1}$$

$$u_s^q(t) = Ri_q(t) + L_q\frac{\mathrm{d}i_q}{\mathrm{d}t} + \omega_{\text{erf}}(t)L_d i_d(t) + \omega_{\text{erf}}(t)\Phi_{\text{mg}}, \tag{2}$$

$$\frac{\omega_{\text{erf}}(t)}{\mathrm{d}t} = \frac{P}{J}T_{\text{em}} - \frac{B}{J}\omega_{\text{erf}}(t) - \frac{P}{J}T_{\text{load}}. \tag{3}$$

The parameters of the IPMSM dynamic model are defined in Table 3.

The electromagnetic torque of the IPMSM can be calculated as [43]

$$T_{\text{em}} = \frac{3}{2}P\left(\Phi_{\text{mg}}i_q(t) + \left(L_d - L_q\right)i_d(t)i_q(t)\right). \tag{4}$$

Remark 1. Due to the nonuniform air-gap flux in the IPMSM, the stator q-inductance L_q is smaller than the stator d-inductance L_d. Opposed to the IPMSM, surface-mounted PMSM is specified by uniform air-gap, and the stator dq-inductances are identical to each other: $L_d = L_q = L_m$[3].

In Figure 3(a), with the assumption of constant DC-bus voltage U_{DC}, equal DC-link capacitors $C_1 = C_2 = C$, and $i^- + i_{abc} = i^+ + i_c$ [44],

$$\frac{\mathrm{d}u_{\text{np}}}{\mathrm{d}t} = \frac{1}{2C}\left(i^+ - i^- - i_{abc}\right) = -\frac{1}{2C}i_c, \tag{5}$$

where $i_{abc} = i_a + i_b + i_c$.

3.2. 3L-SNPC Inverter. The 3L-SNPC inverter consists of a dual Buck converter integrated with a conventional two-level inverter [45]. The 3L-SNPC inverter is supplied by two-series-connected capacities C_1 and C_2 ($C_1 = C_2 = C$). The dual Buck converter consists of four transistors ($S_A - S_D$) with neutral point Z to connect different voltage levels, Table 4, to the input of the two-level inverter. The combinations of the switching states of 3L-SNPC can be calculated by $S_{\text{com}} = S_{2L}S_{\text{DBC}} = 2^3.4 = 32$ combinations, where S_{2L} and S_{DBC} are the switching states of the two-level inverter and dual Buck converter, respectively. The combinations of switching states are devised to 18 active and 14 zero voltage vectors leading to 21 inverter output voltages obtained in abc-coordinate as described in Table 5 [46]. Three groups of voltage vectors are defined: zero voltage vectors VV_Z, small voltage vectors VV_M, and large voltage vectors VV_L.

The topology of the IPMSM fed by 3L-SNPC inverter configuration is depicted in Figure 3(a). In the abc-coordinate, the common-mode voltage u_{cm} measured from the stator winding neutral to neutral point Z is expressed as [47]

$$u_{\text{cm}} = \frac{u_{AZ} - u_{BZ} - u_{CZ}}{3}, \tag{6}$$

where u_{XZ} ($X = A, B, C$) is the phase voltage from an output terminal to neutral point Z.

4. FMPC Formulation

Generally, FMPC generates the optimal switching state by optimizing a predefined cost function, for each possible switching state available in the inverter, that describes the desired system behavior until a predefined

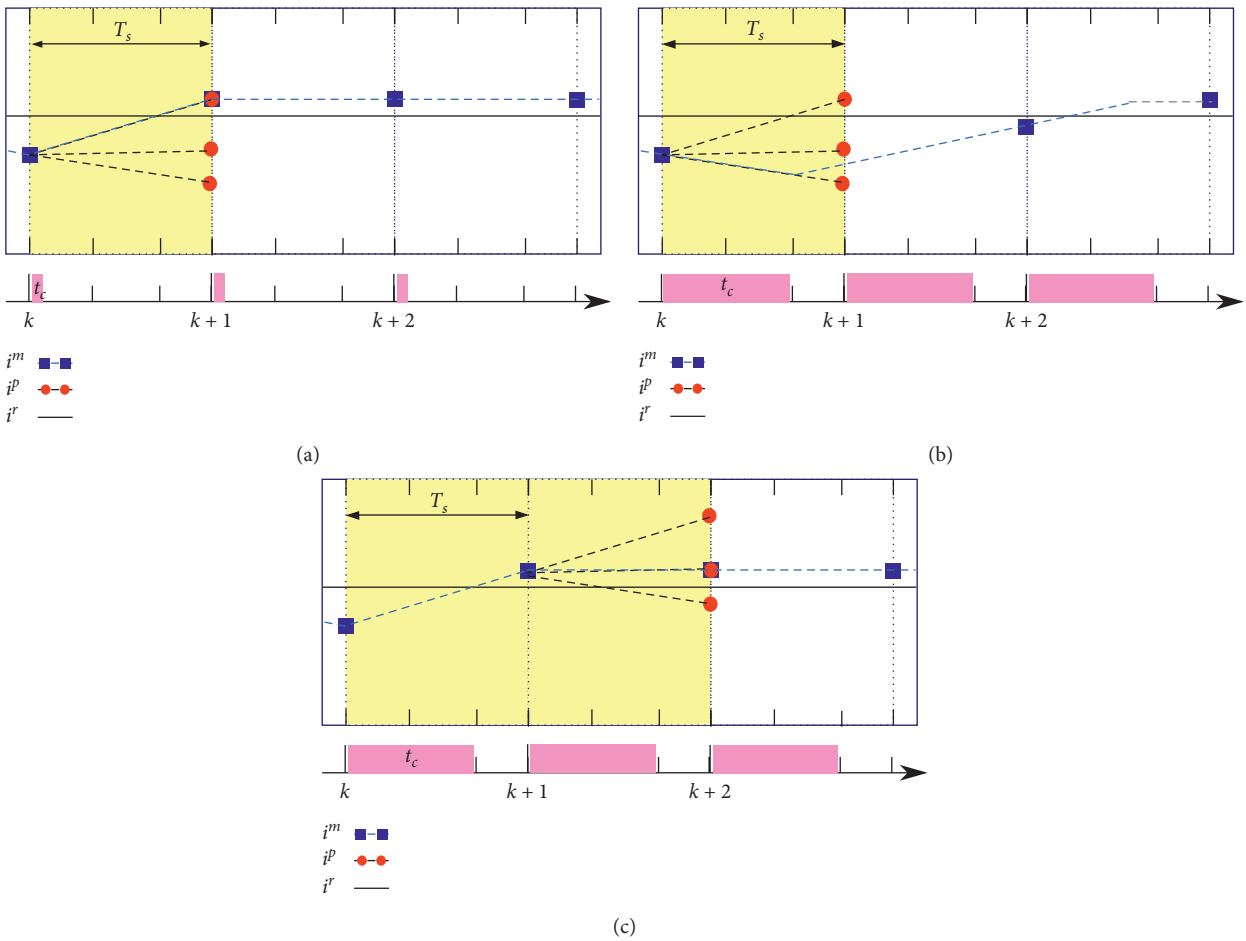

Figure 1: The operating cycle of the FMPC: (a) ideal case: without delay and calculation time t_c is zero; (b) real case: with delay and without compensation and considerable calculation time t_c; (c) real case: with delay and compensation and considerable calculation time t_c.

control horizon. The multiobjective cost function considers the tracking error between the predicted and reference values of controlled variables allowing simultaneous control of all of them. FMPC is a receding horizon approach, namely, its optimization problem is formulated and resolved every sampling period updating the actual system state data.

In general, the cost function consists of two parts: the predicted control errors over the prediction horizon N and the penalty term. Typically, the following quadratic cost function form is used [48]:

$$\Gamma = \sum_{h=t+1}^{t+N} \tilde{y}_h^T \Theta \tilde{y}_h + \sum_{z=t}^{t+N_u} \Delta\tilde{u}_z^T \Pi \Delta\tilde{u}_z, \tag{7}$$

where $\tilde{y}_h = \left\{y_h^p - y_h^r\right\} \in \mathbb{R}^n$ is a vector of error between the predicted and reference values of the controlled variable y at instant h. $\Delta\tilde{u}_z \in \mathbb{R}^m$ is the vector of increments of the future values of the manipulated variable (control inputs) at instant z. N_u and N represent the control and prediction horizons, respectively. Matrices $\Theta \in \mathbb{R}^{n\times n}$ and $\Pi \in \mathbb{R}^{m\times m}$ denote weighting coefficients. Then, the optimal switching state is

$$\mu_{abc}^{\text{opt}} = \arg\left\{\underset{\mu_{abc}^{\text{opt}} \in \{V_1, V_2, \ldots, V_{21}\}}{\text{minimize}} \ \Gamma\right\}. \tag{8}$$

4.1. Cost Function Selection. Cost function designing is one of the most important stages in the definition of any MPC strategy. In this work, the purposes of the proposed predictive control are as follows:

(i) Reducing the mechanical component stress of the IPMSM by fast and accurate reference current tracking

(ii) Limiting the output 3L-SNPC inverter voltage sensibility to the ripples in DC-link voltage by capacitor voltage balancing

(iii) Increasing the safety and reliability of the IPMSM by limiting the peak of common-mode voltage

(iv) Reducing the switching losses by minimizing the switching frequency

When matrices Θ and Π in equation (7) are diagonal, the aforementioned control objectives are included in a single cost function of the FMPC given in the following:

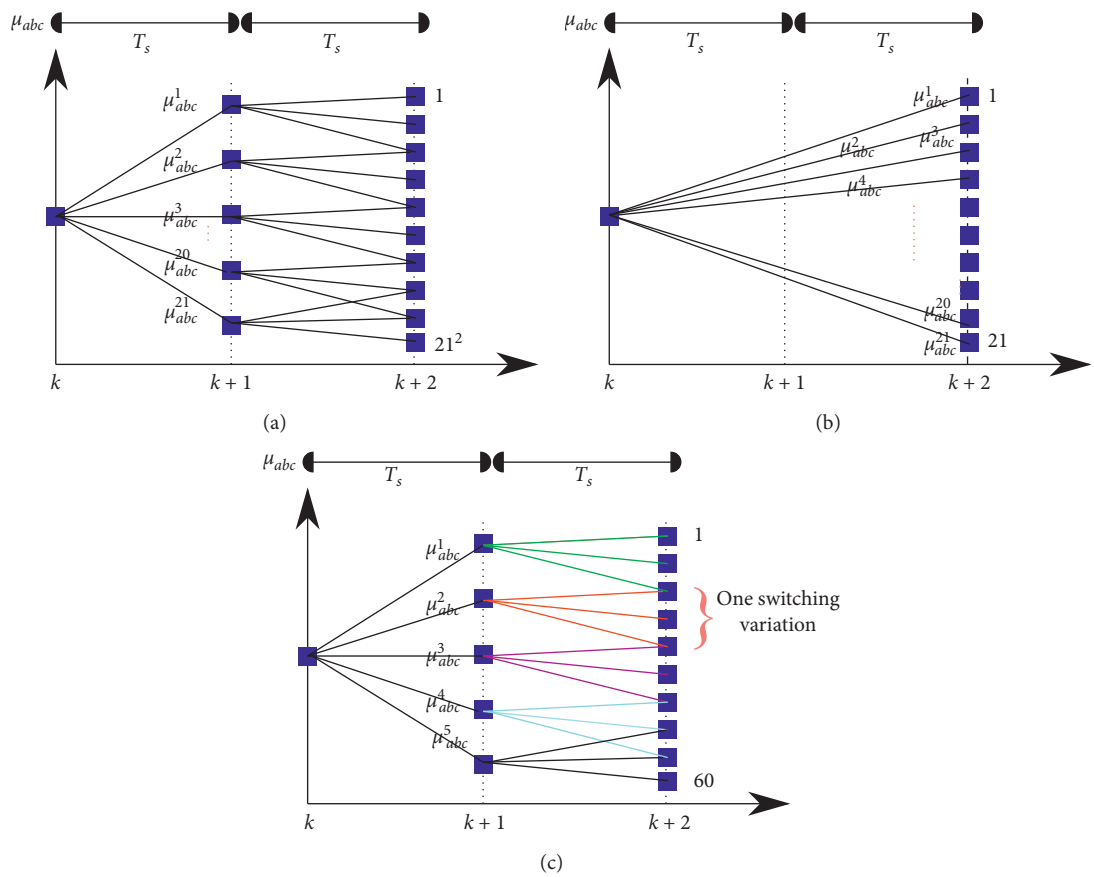

Figure 2: (a) Standard two-step horizon of prediction, (b) modified two-step horizon prediction with the "static voltage vector" (SVV) principle, and (c) modified two-step horizon prediction with the "single state variation" (SSV) principle.

Table 3: IPMSM model parameters.

u_s^{dq}	dq-stator voltages (V)
i^{dq}	dq-stator currents (A)
R	Stator resistance (Ω)
L_{dq}	dq-stator inductances (H)
ω_{erf}	Electric rotatory frequency (rad/s)
Φ_{mg}	Flux linkage (Wb)
T_{em}	Electromagnetic torque (Nm)
T_{load}	External torque (Nm)
P	Number of pole pairs [1]
J	Moment of inertia (kg·m^2)
B	Viscous coefficient (Nm·s)
T_s	Sampling period (s)

$$\Gamma = \Gamma_i + \Gamma_{np} + \Gamma_{cm} + \Lambda_{sw},$$
$$\begin{cases} \Gamma_i = \Lambda_i \left\| i^r(k+1) - i^p(k+1) \right\|^2, \\ \Gamma_{np} = \Lambda_{np} \left\| u^p_{np}(k+1) \right\|^2, \\ \Gamma_{cm} = \Lambda_{cm} \left\| u^p_{cm}(k+1) \right\|^2, \\ \Gamma_{sw} = \Lambda_{sw} \sum_{x=a,b,c} \left| \mu_x(k+1) - \mu_x(k) \right|. \end{cases} \quad (9)$$

The parameters of FMPC cost function are defined in Table 6.

4.2. Weighting Coefficient Design. Cost function (9) synthesizes multiple controlled variables with different natures (e.g., current and voltage), order and magnitude, and effect. Accordingly, the tradeoff between the four controlled variables is defined by the weighting coefficients Λ_i, Λ_{np}, Λ_{cm}, and. Λ_{sw}.

The classification of the cost functions is depended on the controlled variables incorporated in its formulation. Three kinds of cost functions are defined [48]:

(i) Cost function without weighting coefficients: one type of variable is controlled without using the weighting coefficients.

(ii) Cost function with secondary terms: primary goal and secondary constraints are defined to accomplish a proper system behavior and control performances. In this case, the weighting coefficient of the second term is forced to zero ($\Lambda_{st} = 0$). The procedure of tuning the weighting coefficients is converted to the cost function without weighting coefficient procedure. Based on a steady-state error and total harmonic distortion (THD) criteria, the system behavior without the weighting coefficients is evaluated to fulfill the control requirements. Finally, by evaluating the system behavior, the simulation started with $\Lambda_{st} = 0$ and increases progressively

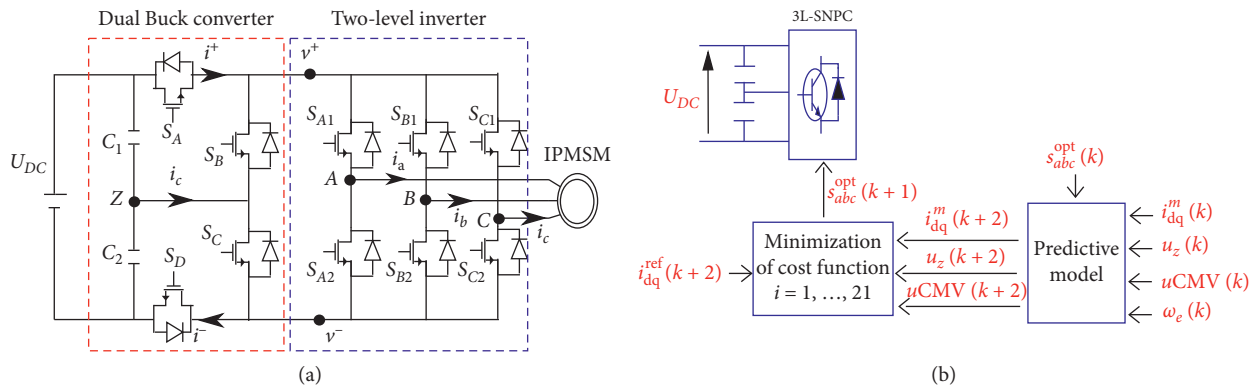

Figure 3: (a) Simplified electrical circuit of the system. (b) Block diagram of the improved FMPC scheme.

Table 4: Operating principle of the 3L-SNPC inverter.

Switching state				Terminal voltage	
S_A	S_B	S_C	S_D	v^+	v^-
ON	OFF	OFF	ON	$+(U_{DC}/2)$	$-(U_{DC}/2)$
ON	OFF	ON	OFF	$+(U_{DC}/2)$	0
OFF	ON	ON	OFF	0	0
OFF	ON	OFF	ON	0	$-(U_{DC}/2)$

Table 5: Switching state combinations of 3L-SNPC.

Order	Switching states	Output voltage		
		u_a	u_b	u_c
I			VV_Z	
V_1	$\{P, P, P\}$	0	0	0
V_2	$\{O, O, O\}$			
V_3	$\{N, N, N\}$			
II			VV_S	
V_4	$\{P, O, O\}$	$U_{DC}/3$	$-(U_{DC}/6)$	$U_{DC}/3$
V_5	$\{O, N, N\}$			
V_6	$\{P, O, O\}$	$U_{DC}/6$	$U_{DC}/6$	$-(U_{DC}/3)$
V_7	$\{O, O, N\}$			
V_8	$\{O, P, O\}$	$-(U_{DC}/6)$	$U_{DC}/3$	$U_{DC}/6$
V_9	$\{N, O, N\}$			
V_{10}	$\{O, P, P\}$	$-(U_{DC}/3)$	$U_{DC}/6$	$U_{DC}/3$
V_{11}	$\{N, O, O\}$			
V_{12}	$\{O, O, P\}$	$-(U_{DC}/6)$	$-(U_{DC}/6)$	$U_{DC}/3$
V_{13}	$\{N, N, O\}$			
V_{14}	$\{P, O, P\}$	$U_{DC}/6$	$-(U_{DC}/3)$	$U_{DC}/6$
V_{15}	$\{O, N, O\}$			
III			VV_L	
V_{16}	$\{P, N, N\}$	$2U_{DC}/3$	$-(U_{DC}/3)$	$-(U_{DC}/3)$
V_{17}	$\{P, P, N\}$	$U_{DC}/3$	$U_{DC}/3$	$-(2U_{DC}/3)$
V_{18}	$\{N, P, N\}$	$-(U_{DC}/3)$	$2U_{DC}/3$	$-(U_{DC}/3)$
V_{19}	$\{N, P, P\}$	$2U_{DC}/3$	$U_{DC}/3$	$U_{DC}/3$
V_{20}	$\{P, P, N\}$	$-(U_{DC}/3)$	$-(U_{DC}/3)$	$2U_{DC}/3$
V_{21}	$\{P, N, P\}$	$U_{DC}/3$	$2U_{DC}/3$	$U_{DC}/3$

until it defined a good tradeoff between the primary goal and secondary constraints. A common approach to select the optimal weighting coefficient is branch and bound technique.

(iii) Cost function with equally important terms: in this case, several variables have equal importance to control the system which are incorporated in the cost function. Firstly, the cost function is normalized. Accordingly, all terms will be similarly important ($\Lambda = 1$). The second and third steps are the same as cost function with secondary terms; $\Lambda = 1$ is considered instead of zero value.

4.2.1. Optimization Algorithm. The discrete-state space model of the IPMSM can be obtained by forward Euler's method using equations (1) and (2) as follows [43]:

$$\begin{bmatrix} i_m^d(k+1) \\ i_m^q(k+1) \end{bmatrix} = \underbrace{\begin{bmatrix} 1-\dfrac{RT_s}{La_d} & T_s\omega_{\mathrm{erf}}(k) \\ -T_s\omega_{\mathrm{erf}}(k) & 1-\dfrac{RT_s}{L_q} \end{bmatrix}}_{\chi_s(k)} \begin{bmatrix} i_m^d(k) \\ i_m^q(k) \end{bmatrix} + \underbrace{\begin{bmatrix} \dfrac{T_s}{L_d} & 0 \\ 0 & \dfrac{T_s}{L_q} \end{bmatrix}}_{\chi_c} \begin{bmatrix} u_s^d(k) \\ u_s^q(k) \end{bmatrix} + \underbrace{\begin{bmatrix} 0 \\ -\dfrac{T_s\Phi_{\mathrm{mg}}(k)}{L_q}\omega_{\mathrm{erf}}(k) \end{bmatrix}}_{\chi_{\mathrm{ft}}(k)}, \tag{10}$$

where $x_m(k) = [i_m^d i_m^q]^T$ and $u_m(k) = [u_s^d u_s^q]^T$ are the stator current and output voltage vectors, respectively, $\chi_s(k)$, χ_c, and $\chi_{ft}(k)$ denote system, input, and feed-through matrices, and T_s is the sampling period.

The future values of reference current are extrapolated using the Lagrange method [49]:

$$i^r(k+1) = 3i^r(k) - 3i^r(k-1) + i^r(k-2). \tag{11}$$

By using equation (5) and actual information of μ_{abc} at the k instance, the predicted value of the neutral-point voltage at the $k+1$ instance is obtained as

$$u_{\mathrm{np}}^p(k+1) = u_{\mathrm{np}}(k) + \frac{T_s}{4C}\left(2|\mu_a(k)| - |\mu_b(k)| - |\mu_c(k)|\right)i_\alpha(k) + \frac{\sqrt{3}T_s}{4C}\left(2|\mu_b(k)| - |\mu_c(k)|\right)i_\beta(k). \tag{12}$$

To compensate the computational delay, according to the long horizon of the prediction approach, we propose to use a two-step horizon of prediction, Section 2.2 and Figure 1. The improved cost function Γ^* with computational delay compensation of improved FMPC (I-FMPC) is evaluated at time $k+2$ to generate the optimal switching state μ_{abc}^{opt} applied at time $k+1$:

$$\begin{aligned} \Gamma^* &= \Gamma_i^* + \Gamma_{\mathrm{np}}^* + \Gamma_{\mathrm{cm}}^* + \Gamma_{\mathrm{sw}}^*, \\ &\begin{cases} \Gamma_i^* = \Lambda_i\left\|i^r(k+2) - i^p(k+2)\right\|^2, \\ \Gamma_{\mathrm{np}}^* = \Lambda_{\mathrm{np}}\left\|u_{\mathrm{np}}^p(k+2)\right\|^2, \\ \Gamma_{\mathrm{cm}}^* = \Lambda_{\mathrm{cm}}\left\|u_{\mathrm{cm}}^p(k+2)\right\|^2, \\ \Gamma_{\mathrm{sw}}^* = \Lambda_{\mathrm{sw}}\sum\limits_{x=a,b,c}\left|\mu_x(k+2) - \mu_x(k+1)\right|. \end{cases} \end{aligned} \tag{13}$$

By using the second-order Lagrange extrapolation, the reference current at the $k+2$ instance is [49]

$$i^r(k+2) = 6i^r(k) - 8i^r(k-1) + 3i^r(k-2). \tag{14}$$

Based on equations (10) and (12), the predicted system state and neutral-point voltage data at the $k+2$ instance are expressed as

$$\begin{aligned} x_m(k+2) &= \chi_s(k+1)x_m(k+1) + \chi_c u_m(k+1) + \chi_{\mathrm{ft}}(k+1), \\ u_{\mathrm{np}}^p(k+2) &= u_{\mathrm{np}}(k+1) + \frac{T_s}{4C}\left(2|\mu_a(k+1)| - |\mu_b(k+1)| - |\mu_c(k+1)|\right)i_\alpha(k+1) + \frac{\sqrt{3}T_s}{4C}\left(2|\mu_b(k+1)| - |\mu_c(k+1)|\right)i_\beta(k+1), \end{aligned} \tag{15}$$

Table 6: FMPC cost function parameters.

Minimization terms	
Γ_i	Current tracking control
Γ_{cm}	Common-mode voltage control
Γ_{np}	Neutral-point voltage control
Γ_{sw}	Reduction of switching frequency
Predicted values	
$i^r(k+1)$	Extrapolated reference current
$u_{\mathrm{np}}^p(k+1)$	Neutral-point voltage
$i^p(k+1)$	Predicted current
$u_{\mathrm{cm}}^p(k+1)$	Common-mode voltage
Weighting coefficients	
Λ_i	Current tracking control
Λ_{cm}	Common-mode voltage control
Λ_{np}	Neutral-point voltage control
Λ_{sw}	Reduction of switching frequency

where $x_m^{\alpha\beta}(k) = [i_m^\alpha i_m^\beta]^T$ is the stator current in $\alpha\beta$-coordinates.

4.3. Stability: Modified Lyapunov Function Constraint. In order to avoid overcurrent/voltage in the power converter and IPMSM, the stator current reference is limited by maximum permissible current I_m and safety factor σ (to reduce the voltage and provide robustness against model uncertainties) [50]:

$$\left\| \left[i_d^r(k) i_q^r(k) \right] \right\| \le I_m, \tag{16}$$

$$\left|\omega_{\mathrm{erf}}\right| \left\| \left[\left(\Phi_{\mathrm{mg}} + L_d i_d^r(k)\right) L_q i_q^r(k) \right] \right\| \le \left(\frac{U_{\mathrm{DC}}}{\sqrt{3}}\right) - \sigma. \tag{17}$$

By taking into account constraints (16) and (17) and the improved cost function with delay compensation (13), optimization problem (8) is converted to

$$\mu_{abc}^{\mathrm{opt}} = \arg\left\{ \underset{\mu_{abc}^{\mathrm{opt}}(k)\in\{N,O,P\}^3, \mu_{abc}^{\mathrm{opt}}(k+1)\in\{N,O,P\}^3}{\text{minimize}} \Gamma^* \right\}, \tag{18a}$$

$$\text{s.t.} \quad x_m(k+i+1) = g\left(x_m(k+i), \mu_{abc}(k+i), \omega_{\mathrm{erf}}(k)\right), \tag{18b}$$

$$x_m(k+i) \in \mathcal{X}_{\mathcal{S}}, \quad i = 0, \ldots, N, \tag{18c}$$

$$\mu_{abc}(k+i) \in \mathcal{U}_{\mathcal{S}}, \quad i = 0, \ldots, N-1. \tag{18d}$$

$\mathcal{X}_{\mathcal{S}}$ and $\mathcal{U}_{\mathcal{S}}$ denote the state and control input constraint sets, respectively. The improved cost function (18a) synthetizes the control objectives for the two-step horizon of prediction. This cost function is evaluated by taking the system constraints into account. The dynamic of the system is fulfilled by (18b) using the measured system state at the k instance. The state and control input constraint sets are implemented by (18c) and (18d), respectively.

The conventional predictive control does not guarantee stability. Accordingly, the modified Lyapunov candidate function (LCF) is proposed to ensure that the neighborhood of the reference signal set $\mathcal{D}_{\mathcal{S}}$ is reached in finite time.

Definition 1. For all $x_m \in \mathcal{X}_{\mathcal{S}} \backslash \mathcal{D}_{\mathcal{S}}$, $\mathcal{X}_{\mathcal{S}} = \mathbb{R}^n$, there exists a preliminary LCF $\Upsilon(x_m) \ge 0$, $\mu_{abc} \in \mathcal{U}_{\mathcal{S}}$, $\eta > 0$, and $\rho(k) > 0$:

$$\Upsilon\left(g\left(x_m, \mu_{abc}, \omega_{\mathrm{erf}}\right)\right) \le \max\left(\Upsilon(x_m) - \rho(k), \eta\right), \tag{19}$$

where η is a tuning parameter used to compromise the controlled variables.

Proof 1. For every $x_m \in \mathcal{X}_{\mathcal{S}}$, there exists an admissible input such that $x_m + \mu_{abc} \in \mathcal{D}_{\mathcal{S}}$, i.e., $\exists \mu_{abc} \in \mathcal{U}_{\mathcal{S}}$:

$$\Upsilon(x_m + \mu_{abc}) - \left(\frac{1}{\sqrt{3}}\right) \le 0, \quad \forall x_m \in \mathcal{X}_{\mathcal{S}}. \tag{20}$$

$\mathcal{D}_{\mathcal{S}}$ is the convex control set and is defined as the convex hull $\mathfrak{H}_{\ell}$ of $\mathcal{U}_{\mathcal{S}}$ [38]:

$$\mathcal{D}_{\mathcal{S}} \overset{\mathrm{def}}{=} \mathrm{hull}\, \mathcal{U}_{\mathcal{S}} = \left\{ \nu \in \mathbb{R}^2 \,\middle|\, \mathfrak{H}_{\ell} \le \left(\frac{1}{\sqrt{3}}\right) \right\}. \tag{21}$$

ν is the sum of the feedback controller $u \in \mathcal{U}_{\mathcal{S}}$.

Definition 2. Considering η parameter, $\mathcal{D}_{\mathcal{S}}$ is a sublevel set of the LCF:

$$\mathcal{D}_{\mathcal{S}} = \{x_m \colon \Upsilon(x_m) \le \eta\} \subset \mathcal{X}_{\mathcal{S}}. \tag{22}$$

Due to the discrete nature of the 3L-SNPC inverter, the controlled variable cannot always achieve its reference value, namely, the capacity of the controlled system state x_m towards the origin by feasible inputs $\mu_{abc} \in \mathcal{U}_{\mathcal{S}} = \{V_1, V_2, \ldots, V_{21}\}$ is limited.

Proposition 1. *To describe how fast the LCF decreases beyond a certain value, we define*

$$\rho(k) \in \left(\left(\frac{(0,1)}{\sqrt{3}}\right) - \Upsilon\left(\tilde{i}_{\mathrm{dq}}\right)\right). \tag{23}$$

$\rho(k)$ has a direct effect on the LCF performances; if $\rho(k)$ is fixed as a large value, LCF decreases faster, and the algorithm robustness against the model uncertainties is improved. Accordingly, equation (18c) is implemented in the predictive problem formulation as a stabilizing constraint to ensure the recursive feasibility in the problem optimization by the finite-time convergence of the system states to the set $\mathcal{D}_{\mathcal{S}}$.

In equation (23), the dynamic of the current error $\tilde{i}_{\mathrm{dq}} = [\tilde{i}_d, \tilde{i}_q]$ is defined as the difference between the reference and actual stator current:

$$\tilde{i}_{\mathrm{dq}} = \begin{bmatrix} i_d^m(k) \\ i_q^m(k) \end{bmatrix} - \begin{bmatrix} i_d^r(k) \\ i_q^r(k) \end{bmatrix}. \tag{24}$$

The proposed modified LCF in this work is defined as

$$\Upsilon\left(g\left(x_m, \mu_{abc}, \omega_{\mathrm{erf}}\right)\right) \le \max\left(\Upsilon(x_m) + \nu(k) - \rho(k), \eta\right). \tag{25}$$

Proposition 2. *The time-varying function $\nu(k) \ge 0$ is proposed as*

$$\nu(k+j) = 0, \quad \forall j \ge \kappa_1,\ \kappa_1 \in \mathbb{Z}_+. \tag{26}$$

κ_1 is a time instant when the modified LCF constraint suits the standard one. Conditioned by the constraint in equation (18c) is relaxed, the recursive feasibility of the proposed control is guaranteed regardless of the cost function.

By considering (19), the value of the LCF can be decreased robustly for all $(x_m \in \mathbb{R}^2)\backslash\mathscr{D}_{\mathcal{S}}$. Consequently, any x_m state is driven towards the $\mathscr{D}_{\mathcal{S}}$ set. In addition, for all $x_m \in \mathscr{X}_{\mathcal{S}}$ there exists $\mu_{a,b,c} \in \mathscr{U}_{\mathcal{S}}$ when $x_m + \mu_{a,b,c} \in \mathscr{D}_{\mathcal{S}}$. Consequently, there exists a sequence $\mu_{a,b,c}(0), \mu_{a,b,c}(T_s), \ldots, \mu_{a,b,c}(kT_s), \ldots, \in \mathscr{U}_{\mathcal{S}}$ such that

$$\lim_{k\longrightarrow+\infty} x_m(kT_s) \in \mathscr{D}_{\mathcal{S}} \stackrel{\text{def}}{=} \mathscr{D}_{\mathcal{S}}. \tag{27}$$

The FMPC system is said to be global and robust asymptotically set stabilizable.

Proposition 3. *Using the specific structure of the $\mathscr{D}_{\mathcal{S}}$ and $\mathscr{U}_{\mathcal{S}}$ sets, the largest set Υ is*

$$\Upsilon = \left\{ u \in \mathbb{R}^2 \,\middle|\, \mathfrak{H}_u \le \eta + \frac{1}{\sqrt{3}} - \left(\frac{1}{\sqrt{3}} - \rho\right) \right\}. \tag{28}$$

Therefore, the modified LCF is

$$\Upsilon\left(\tilde{i}_d, \tilde{i}_q\right) = \frac{1}{2}\Psi_d \tilde{i}_d^2 + \frac{1}{2}\Psi_q \tilde{i}_q^2, \tag{29}$$

with

$$\Delta\Upsilon = \Upsilon\left(\tilde{i}_d^p(k+1), \tilde{i}_q^p(k+1)\right) - \Upsilon\left(\tilde{i}_d(k), \tilde{i}_q(k)\right), \tag{30}$$

where Ψ_d and Ψ_q are the positive gains.

Considering the modified LCF (29) and (30) in improved cost function (18b), the following modified I-FMPC (MI-FMPC) is proposed:

$$\mu_{abc}^{\text{opt}} = \arg\left\{ \underset{\mu_{abc}^{\text{opt}}(k)\in\{N,O,P\}^3, \mu_{abc}^{\text{opt}}(k+1)\in\{N,O,P\}^3}{\text{minimize}} \Gamma^* \right\}, \tag{31a}$$

$$\text{s.t.} \quad x_m(k+i+1) = g\left(x_m(k+i), \mu_{abc}(k+i), \omega_{\text{erf}}(k)\right), \tag{31b}$$

$$x_m(k+i) \in \mathscr{X}, \quad i = 0, \ldots, N, \tag{31c}$$

$$\mu_{abc}(k+i) \in \mathscr{U}, \quad i = 0, \ldots, N-1, \tag{31d}$$

$$\left((\Upsilon(k) > \varepsilon_\Upsilon) \& (\Delta\Upsilon < 0)\right) \vee \left((\Upsilon(k) < \varepsilon_\Upsilon) \& (\Upsilon(k+1) < \varepsilon_\Upsilon)\right). \tag{31e}$$

It can be shown that, in predictive problem formulation (31a), the modified LCF stability criteria constraint is imposed with (31e). With the aim to ensure the stability of the closed loop, the switching states μ_{abc}^j, $j \in \{1, 2, \ldots, 21\}$ which violate the constraints are discarded, while the remaining states are compared according to the cost function. Two cases are considered: the first one corresponds to $\Upsilon(k) > \varepsilon_\Upsilon$ and the second one $\Upsilon(k) > \varepsilon_\Upsilon$. If $\Upsilon(k) > \varepsilon_\Upsilon$, only switches obtaining $\Delta\Upsilon < 0$ are considered, and if $\Upsilon(k) > \varepsilon_\Upsilon$, only switches assuring $\Upsilon(k+1) > \varepsilon_\Upsilon$ are considered. Hence, ε_Υ can be used as a stabilizing constraint that guarantees recursive feasibility and stability for the optimization problem.

A simplified algorithm of the proposed MI-FMPC is summarized in Algorithm 1.

5. Proposed Computationally Efficient MI-FMPC Algorithms

As mentioned in Section 2.3, an amount of $21^2 = 441$ iterations is required to evaluate the improved cost function (31a) which makes a challenge in MI-FMPC algorithm implementation. To overcome this issue, in this work, the MI-FMPC in (31a) is developed with two proposed computation-efficient principles: "static voltage vector" (SVV), Figure 2(b), and "single state variation" (SSV), Figure 2(c). It is worth to state that the "SVV" and "SSV" principles are based on the approach of limiting the evaluation of cost function (31a) in case of a long horizon of a prediction, and they are applied separately to the proposed computationally efficient MI-FMPC (CMI-FMPC) strategy.

5.1. Computationally Efficient MI-FMPC-SVV. In order to reduce the computational burden, the proposed static voltage vector (SVV) principle is based on the evaluation of (32a) using fixed vector voltage during the two-step horizon of prediction instead of different voltage vectors, Figure 2(b). In computationally efficient MI-FMPC-SVV (CMI-FMPC-SVV) formulation in (32a), the "SVV" principle is implemented using constraint (32f):

$$\mu_{abc}^{\text{opt}} = \arg\left\{ \underset{\mu_{abc}^{\text{opt}}(k)\in\{N,O,P\}^3, \mu_{abc}^{\text{opt}}(k+1)\in\{N,O,P\}^3}{\text{minimize}} \Gamma^* \right\}, \tag{32a}$$

$$\text{s.t.} \quad x_m(k+i+1) = g\left(x_m(k+i), \mu_{abc}(k+i), \omega_{\text{erf}}(k)\right), \tag{32b}$$

$$x_m(k+i) \in \mathscr{X}, \quad i = 0, \ldots, N, \tag{32c}$$

$$\mu_{abc}(k+i) \in \mathscr{U}, \quad i = 0, \ldots, N-1, \tag{32d}$$

$$\left((\Upsilon(k) > \varepsilon_\Upsilon) \& (\Delta\Upsilon < 0)\right) \vee \left((\Upsilon(k) < \varepsilon_\Upsilon) \& (\Upsilon(k+1) < \varepsilon_\Upsilon)\right), \tag{32e}$$

$$\mu_{abc}(k) = \mu_{abc}(k+1). \tag{32f}$$

The simplified algorithm of the proposed CMI-FMPC-SVV is presented in Algorithm 2. The two loops depicted in the predictive control formulation presented in Algorithm 1 are embarked in a single loop in Algorithm 2.

5.2. Computationally Efficient MI-FMPC-SSV. To avoid the high computational burden in two-step horizon of prediction in (31a) formulation of the proposed MI-FMPC strategy, the single state variation (SSV) principle is proposed, namely, in the first stage of prediction, the 21 system states $x_m(k+1)$ are predicted. In the second stage, the transition of the switching state is limited to the combinations of inputs that have only one state variation in $k+2$, Figure 2(c). For example, if the vector voltage

Require: $i_{dq}^{m}(k), i_{dq}^{r}(k)$, $u_{np}(k)$, $u_{cm}(k)$, $\omega_{erf}(k)$;
  Extrapolation of references $i_{dq}^{r}(k+1)$ and $i_{dq}^{r}(k+2)$;
  % Initialize the values of μ_{abc}^{opt} and Γ^{*};
  Set $\mu_{abc}^{opt} = 1$; $\Gamma^{*} = \text{zeros}(21{:}\ 21)$;
  for $i = 1:21$ **do**
    Compute predictions: $u_{dq}^{s}(k+1)$ and $i_{dq}^{p}(k+1)$;
    Calculate the current error $\tilde{i}_{dq}$;
    Evaluate the Lyapunov candidate function: $\Upsilon(k+1)$, $\Upsilon(k)$, $\Delta\Upsilon(k)$;
    if $((\Upsilon(k) > \varepsilon_{\Upsilon})\&(\Delta\Upsilon < 0)) \vee ((\Upsilon(k) < \varepsilon_{\Upsilon})\&(\Upsilon(k+1) < \varepsilon_{\Upsilon}))$ **then**
      Prediction of $u_{np}^{p}(k+1)$ and $u_{cm}^{p}(k+1)$;
      for $j = 1:21$ **do**
        Predict $u_{dq}^{s}(k+2)$, $i_{dq}^{p}(k+2)$, $u_{np}^{p}(k+2)$ and $u_{cm}^{p}(k+2)$;
        Estimate $|\mu_{abc}^{j}(k+2) - \mu_{abc}^{opt}(k+1)|$;
        Evaluate and store the cost function $\Gamma^{*}(i, j)$ value;
      end for
    end if
  end for
  Select and apply the optimal switching state $\mu_{abc}^{opt} = \min(\Gamma^{*})$;

Algorithm 1: Proposed MI-FMPC.

Require: $i_{dq}^{m}(k), i_{dq}^{r}(k)$, $u_{np}(k)$, $u_{cm}(k)$, $\omega_{erf}(k)$;
  Extrapolation of references $i_{dq}^{r}(k+1)$ and $i_{dq}^{r}(k+2)$;
  % Initialize the values of μ_{abc}^{opt} and Γ^{*};
  Set $\mu_{abc}^{opt} = 1$; $\Gamma^{*} = \text{zeros}(1{:}\ 21)$;
  for $i = 1:21$ **do**
    Compute predictions: $u_{dq}^{s}(k+1)$ and $i_{dq}^{p}(k+1)$;
    Calculate the current error $\tilde{i}_{dq}$;
    Evaluate the Lyapunov candidate function: $\Upsilon(k+1)$, $\Upsilon(k)$, $\Delta\Upsilon(k)$;
    if $((\Upsilon(k) > \varepsilon_{\Upsilon})\&(\Delta\Upsilon < 0)) \vee ((\Upsilon(k) < \varepsilon_{\Upsilon})\&(\Upsilon(k+1) < \varepsilon_{\Upsilon}))$ **then**
      Prediction of $u_{np}^{p}(k+1)$ and $u_{cm}^{p}(k+1)$;
      Predict $u_{dq}^{s}(k+2)$, $i_{dq}^{p}(k+2)$, $u_{np}^{p}(k+2)$ and $u_{cm}^{p}(k+2)$;
      Estimate $|\mu_{abc}^{j}(k+2) - \mu_{abc}^{opt}(k+1)|$;
      Evaluate and store the cost function $\Gamma^{*}(1, i)$ value;
    end if
  end for
  Select and apply the optimal switching state $\mu_{abc}^{opt} = \min(\Gamma^{*})$;

Algorithm 2: Proposed CMI-FMPC-SVV.

$V_{10} = \{O, P, P\}$ is considered in the first stage, the voltage vectors considered in the second stage are $V_{10} = \{O, P, P\}$, $V_{19} = \{N, P, P\}$, $V_{1} = \{P, P, P\}$, $V_{12} = \{O, O, P\}$, and $V_{8} = \{O, P, O\}$, Table 5. The "SSV" principle constraint is implemented in proposed CMI-FMPC-SSV formulation (33a) using constraint (33f):

$$\mu_{abc}^{opt} = \arg\left\{ \underset{\mu_{abc}^{opt}(k)\in\{N,O,P\}^{3},\mu_{abc}^{opt}(k+1)\in\{N,O,P\}^{3}}{\text{minimize}} \Gamma^{*} \right\}, \tag{33a}$$

$$\text{s.t.} \quad x_{m}(k+i+1) = g\left(x_{m}(k+i), \mu_{abc}(k+i), \omega_{erf}(k)\right), \tag{33b}$$

$$x_{m}(k+i) \in \mathcal{X}, \quad i = 0, \ldots, N, \tag{33c}$$

$$\mu_{abc}(k+i) \in \mathcal{U}, \quad i = 0, \ldots, N-1, \tag{33d}$$

$$\left((\Upsilon(k) > \varepsilon_{\Upsilon})\&(\Delta\Upsilon < 0)\right) \vee \left((\Upsilon(k) < \varepsilon_{\Upsilon})\&(\Upsilon(k+1) < \varepsilon_{\Upsilon})\right), \tag{33e}$$

$$\left\|\mu_{abc}(k) - \mu_{abc}(k+1)\right\| < 1. \tag{33f}$$

The simplified algorithm of the proposed CMI-FMPC-SSV is illustrated in Algorithm 3.

Remark 2. The weighting coefficients Λ_{i}, Λ_{np}, Λ_{cm}, and Λ_{sw} are tuned in a "trial-and-error" manner.

6. Simulation and Comparisons

In order to verify the performances of the proposed predictive controls, a comparative study based on numerical simulations of proposed CMI-FMPC-SVV and proposed

Require: $i_{dq}^{m}(k), i_{dq}^{r}(k), u_{np}(k), u_{cm}(k), \omega_{erf}(k)$;
  Extrapolation of references $i_{dq}^{r}(k+1)$ and $i_{dq}^{r}(k+2)$;
  % Initialize the values of μ_{abc}^{opt} and Γ^{*};
  Set $\mu_{abc}^{opt} = 1$; $\Gamma^{*} = \text{zeros}(21{:}\ \alpha)$;
  for $i = 1:21$ **do**
    Compute predictions: $u_{dq}^{s}(k+1)$ and $i_{dq}^{p}(k+1)$;
    Calculate the current error $\tilde{i}_{dq}$;
    Evaluate the Lyapunov candidate function: $\Upsilon(k+1), \Upsilon(k), \Delta\Upsilon(k)$;
    if $((\Upsilon(k) > \varepsilon_{\Upsilon})\&(\Delta\Upsilon < 0)) \vee ((\Upsilon(k) < \varepsilon_{\Upsilon})\&(\Upsilon(k+1) < \varepsilon_{\Upsilon}))$ **then**
      Prediction of $u_{np}^{p}(k+1)$ and $u_{cm}^{p}(k+1)$;
      Corresponding combination switching states having a difference of one switch α;
      for $j = 1{:}\ \alpha$ **do**
        Predict $u_{dq}^{s}(k+2)$, $i_{dq}^{p}(k+2)$, $u_{np}^{p}(k+2)$ and $u_{cm}^{p}(k+2)$;
        Estimate $|\mu_{abc}^{j}(k+2) - \mu_{abc}^{opt}(k+1)|$;
        Evaluate and store the cost function $\Gamma^{*}(i, \alpha)$ value;
      end for
    end if
  end for
  Select and apply the optimal switching state $\mu_{abc}^{opt} = \min(\Gamma^{*})$;

Algorithm 3: Proposed CMI-FMPC-SSV.

CMI-FMPC-SSV strategies for IPMSM fed by the 3L-SNPC multilevel inverter is presented in this section. The proposed system and control schemes which are presented in Figure 3 are carried out using Matlab/Simulink software and SimPowerSystems toolbox with parameters detailed in Table 7. Figures 4–6 show the simulation results of the behavior of the controlled variables.

Remark 3. In this section and for clarity purposes, both proposed CMI-FMPC-SVV and CMI-FMPC-SSV predictive strategies are indicated by SVV and SVV abbreviations in the simulation figures, respectively.

6.1. Steady-State Performances. The reference, predicted, and measured stator current values are illustrated in Figure 4(a). Both measured currents i^{SVV} and i^{SVV} can accurately track their reference values, and good tracking performance can be reached by both proposed predictive algorithms. The behavior of proposed predictive strategies is illustrated in Figure 4(b). The current error η^{SVV} obtained with the proposed CMI-FMPC-SVV is less than the error obtained by using CMI-FMPC-SSV, ηSSV, where $\eta = i^{r} - i^{m}$.

With the aim to better study the steady-state performances of the proposed predictive controls, we propose to use the tracking error [40]:

$$\overset{\circ}{e}(y) = \frac{1}{Q}\sum_{j=1}^{Q}\left|\frac{y^{r}(j) - y^{m}(j)}{y^{r}(j)}\right|. \tag{34}$$

Q determined the number of simulation iterations during the simulation. y^{m} and y^{r} are measured and reference controlled variables of y, respectively. The calculated tracking error of the controlled variables $\overset{\circ}{e}(i_{dq})$, $\overset{\circ}{e}(u_{np})$, and $\overset{\circ}{e}(u_{cm})$ is depicted in Table 8. From these results, the proposed CMI-FMPC-SVV obtains accurate controlled variable tracking ability better than the proposed CMI-FMPC-SSV predictive strategy.

The behavior of output inverter voltage, common-mode voltage, and neutral-point voltage is depicted in Figures 5(c)–5(f) and 6, respectively. Figure 6 shows the good ability to balance the neutral-point voltage by the proposed CMI-FMPC-SVV which is better than the proposed CMI-FMPC-SSV.

6.2. Dynamic-State Performances. The dynamic-state performances of proposed CMI-FMPC-SVV and proposed CMI-FMPC-SSV predictive controls are illustrated in Table 9. As shown in Figure 4(a), the proposed predictive strategies present good dynamic-state performances with settling times of 1.1 ms and 2.5 ms, respectively, and without overshoot and undershoot. The proposed "static voltage vector" (SVV) principle significantly improves the dynamic performance of the predictive strategy compared with the proposed "single state variation" (SSV) principle.

The *tic/toc* Matlab command returns the execution time τ taken to run the proposed predictive algorithms. τ_{max}, τ_{mean}, and τ_{min} are the maximum, average, and minimum execution time required by iteration for the proposed predictive strategies which are presented in Table 10, respectively. The average τ_{mean} of the proposed CMI-FMPC-SVV control is 17.421 μs, in contrast to the CMI-FMPC-SSV strategy of 21.38 μs. It is noted that the computation time of the proposed CMI-FMPC-SVV is reduced by $1 - (21/60) = 0.35$ to 65% of the proposed CMI-FMPC-SSV; 21 and 60 are

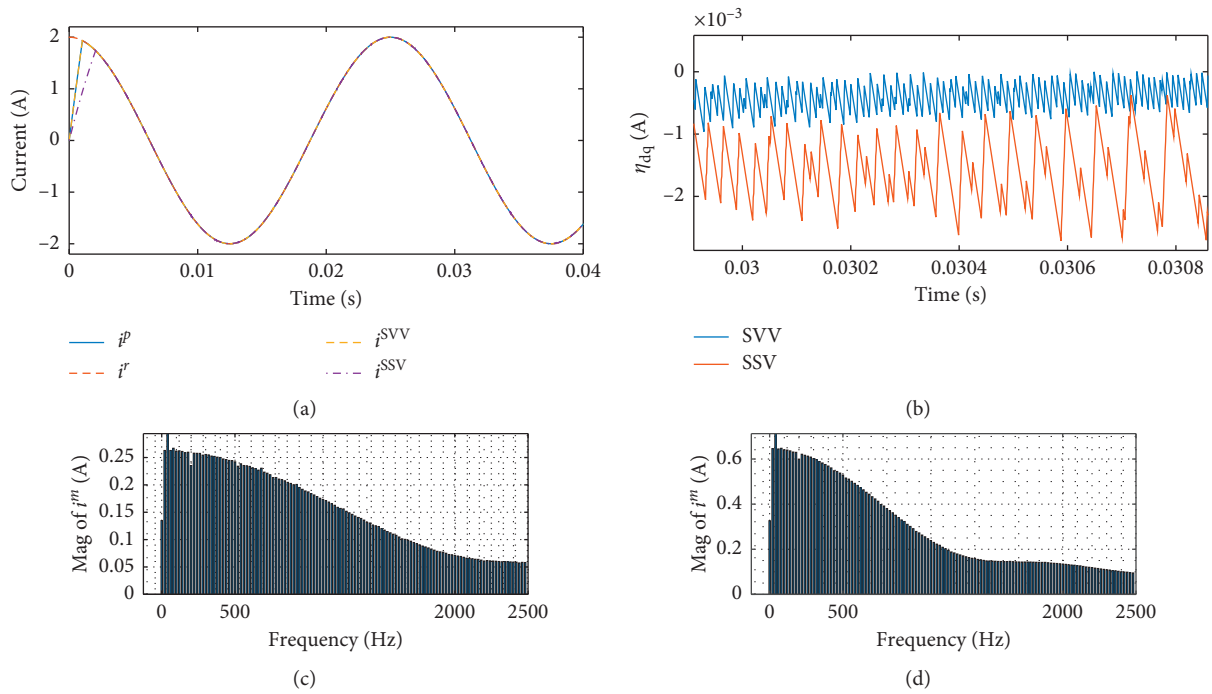

Figure 4: (a) Predicted, reference, and measured i^{SVV} and i^{SSV} stator currents. (b) η^{SVV} and η^{SVV} stator current errors. (c) THD (i_m^{SVV}), fundamental (40 Hz) = 1.995, THD = 2.01%. (d) THD (i_m^{SVV}), fundamental (40 Hz) = 1.989, THD = 3.93%.

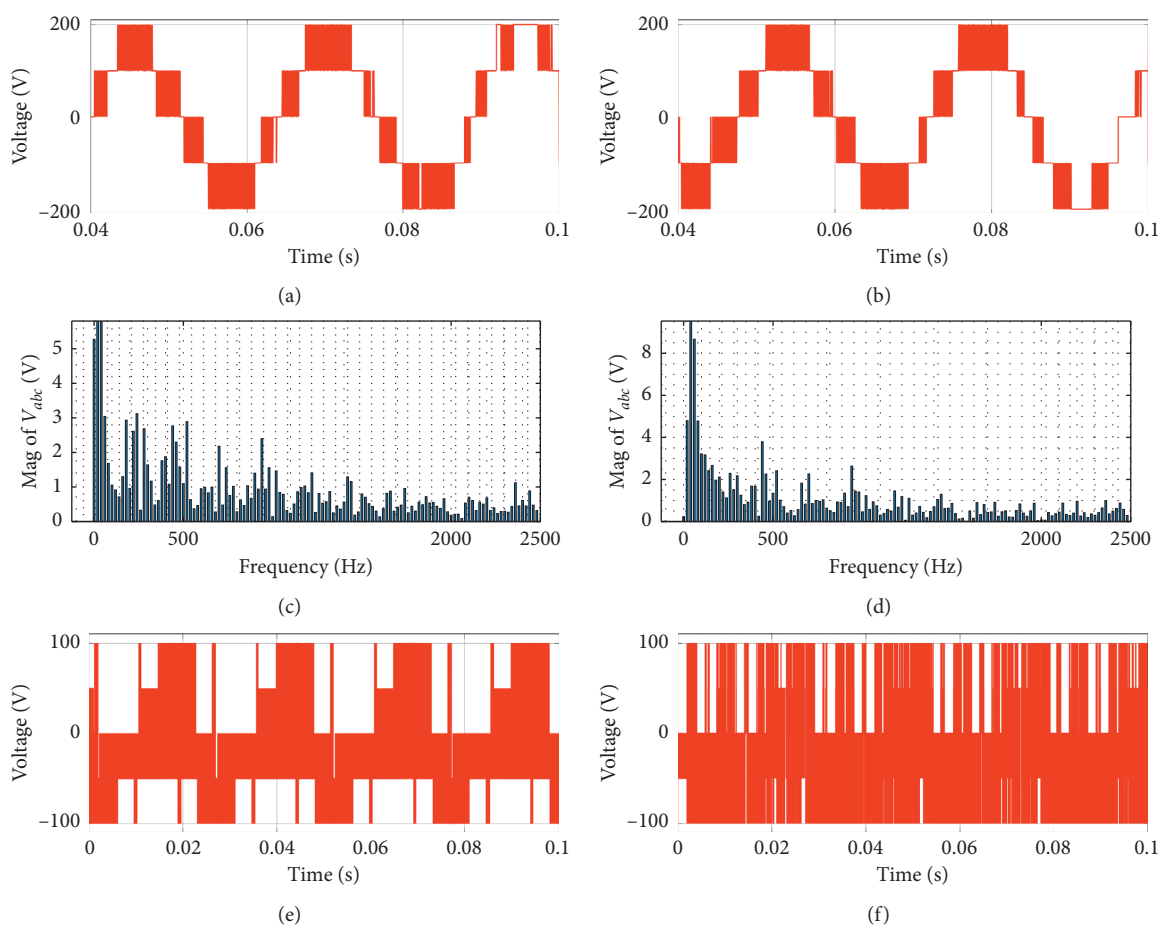

Figure 5: Continued.

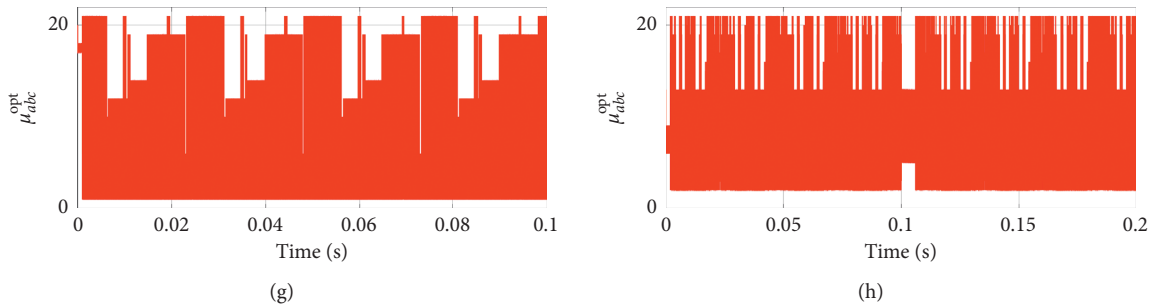

Figure 5: (a) u_a^{SVV}. (b) u_a^{SVV}. (c) THD (u_a^{SVV}), fundamental (40 Hz) = 186.7, THD = 26.26%. (d) THD (u_a^{SVV}), fundamental (40 Hz) = 180.1, THD = 29.91%. (e) u_{cm}^{SVV}. (f) u_{cm}^{SVV}. (g) sw^{SVV}. (h) sw^{SVV}.

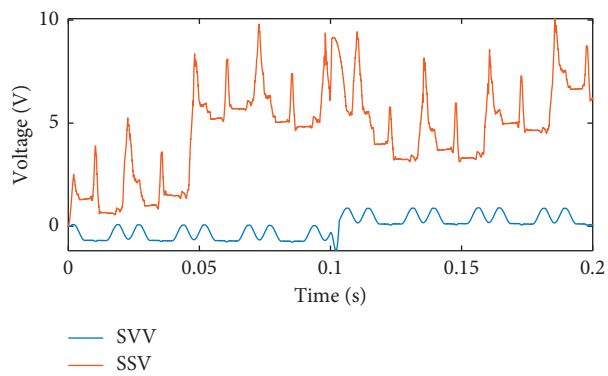

Figure 6: The behavior of neutral-point voltages u_{np}^{SVV} and u_{np}^{SVV}.

Table 7: System parameters.

Parameter	Value
Power rate, P_N (KW)	1.5
Pole pairs, P [1]	2
Resistance, $R(\Omega)$	4.9
DC-link voltage, U_{DC} (V)	300
Flux linkage, Φ_{mg} (Wb)	0.125
d-inductance, L_d (mH)	381
q-inductance, L_q (mH)	873
DC capacitance, $C_1 = C_2 = C$ (μF)	200

the iteration numbers in the second stage of prediction in Figures 2(b) and 2(c).

6.3. Total Harmonic Distortion (THD). To evaluate the effect of the proposed predictive controls on the quality of stator current and output inverter voltage, the Powergui toolbox in Simulink is used to calculate the THD of both of them, Figures 4(c), 4(d), 5(c), and 5(d). The results illustrated in Table 11 indicate that the THD of the proposed CMI-FMPC-SVV is better than the proposed CMI-FMPC-SSV control.

6.4. Switching Frequency. The FMPC predictive strategy generates the optimal switching states μ_{abc}^{opt} with a variable-switching frequency procedure. To analyse the effect of the two proposed predictive strategies on the switching

Table 8: Steady-state performances.

Predictive strategy	$\mathring{e}$ (i_{dq})	$\mathring{e}$ (u_{np})	$\mathring{e}$ (u_{cm})
Proposed CMI-FMPC-SVV	0.0113	0.6002	−0.0417
Proposed CMI-FMPC-SSV	0.0211	−41.2603	4.6115

Table 9: Dynamic-state performances.

Predictive strategy	Proposed CMI-FMPC-SVV	Proposed CFI-FMPC-SSV
Rise time (ms)	1.033	2.52
Settling time (ms)	1.1	2.5
Overshoot (%)	0	0
Undershoot (%)	0	0

frequency, we propose to use the average switching number per semiconductor factor [49]:

$$\breve{f}_{sw} = \frac{1}{Q}\sum_{k=1}^{Q}\frac{sw_{ij}(k)}{10} = \frac{1}{Q}\sum_{k=1}^{Q}\frac{\left|s_{ij}(k+1) - s_{ij}(k)\right|}{10}. \quad (35)$$

The average switching number per semiconductor factor of proposed CMI-FMPC-SVV and proposed CMI-FMPC-SSV predictive strategies is listed in Table 12. The proposed CMI-FMPC-SVV reduces the switching frequency by 1 − (13381/30561) = 0.5622 to 43.78% of the proposed CMI-FMPC-SSV control.

Table 10: Execution time $\tau(\mu s)$.

Predictive strategy	τ_{min}	τ_{mean}	τ_{max}
Proposed CMI-FMPC-SVV	10.5	17.421	22.4
Proposed CMI-FMPC-SSV	16.3	21.38	59.8

Table 11: The current spectra and THD.

Predictive strategy	THD (i_{dq}^{m})	THD (u_s)
Proposed CMI-FMPC-SVV	2.01	26.26
Proposed CMI-FMPC-SSV	3.93	29.91

Table 12: Switching frequency $\breve{f}_{sw}$.

Predictive strategy	Proposed CMI-FMPC-SVV	Proposed CMI-FMPC-SSV
$\breve{f}_{sw}$	13,381	30,561

7. Conclusion and Future Work

In this paper, a novel scheme of predictive control has been proposed and applied to the interior permanent magnet synchronous motor (IPMSM) driven by a three-level simplified neutral-point clamped inverter (3L-SNPC) for electric vehicle applications (EVAs). The main advantages of the novel scheme are summarized as follows: firstly, using a two-step horizon of prediction, the computational delay is compensated. The delay compensation is adopted with a 3L-SNPC inverter structure. Secondly, the stability and feasibility of the proposed predictive control are guaranteed using a modified control Lyapunov function. Thirdly, the computational burden is reduced by applying the proposed "static voltage vector" (SVV) and "single state variation" (SSV) principles. Fourthly, the aforementioned concepts are combined in the predictive problem formulation as additional constraints without sacrificing the simplicity and performances of the controller structure. The simulation results demonstrated that the proposed CMI-FMPC-SVV outperforms the proposed CMI-FMPC-SSV in terms of: good tracking performance, low tracking error of controlled variables, and reduced computational burden and switching frequency by 35% and 56.22%, respectively. The conservatism introduced by using a conventional Lyapunov function constraint can be alleviated by using the proposed modified Lyapunov function constraint which enables nonmonotone convergence to the terminal set and therefore can lead to better performance. The main challenge in this study is the selection of suitable weighting factors in the cost function to achieve the optimal balance between the objectives. To avoid the time and effort consuming simulations in weighting factor selection processes, the future work proposes to use an Artificial Neural Network (ANN) to select the optimal weighting factors in the MPC cost function.

Data Availability

No data were used to support this study.

Conflicts of Interest

The authors declare that there are no conflicts of interest regarding the publication of this paper.

References

[1] X. Gao, B. Sun, X. Hu, and K. Zhu, "Echo state network for extended state observer and sliding mode control of vehicle drive motor with unknown hysteresis nonlinearity," *Mathematical Problems in Engineering*, vol. 2020, Article ID 2534038, 13 pages, 2020.

[2] L. Sheng, D. Li, and Y. Ji, "Two-vector FCS-MPC for permanent-magnet synchronous motors based on duty ratio optimization," *Mathematical Problems in Engineering*, vol. 2018, Article ID 9061979, 9 pages, 2018.

[3] P. Gao, G. Zhang, H. Ouyang, and L. Mei, "A sliding mode control with nonlinear fractional order PID sliding surface for the speed operation of surface-mounted PMSM drives based on an extended state observer," *Mathematical Problems in Engineering*, vol. 2019, Article ID 7130232, 13 pages, 2019.

[4] Y.-H. Lan and L. Zhou, "Backstepping control with disturbance observer for permanent magnet synchronous motor," *Journal of Control Science and Engineering*, vol. 2018, Article ID 4938389, 8 pages, 2018.

[5] L. Mo, Y. Liu, and Y. Zhang, "Sliding mode variable structure control for surface permanent magnet synchronous motors based on a fuzzy exponential reaching law," *Mathematical Problems in Engineering*, vol. 2019, Article ID 8340956, 14 pages, 2019.

[6] A. Katkout, A. Essadki, and T. Nasser, "Nonlinear power control strategies for variable-speed wind turbines," *International Journal of Renewable Energy Research (IJRER)*, vol. 7, no. 4, pp. 1998–2003, 2017.

[7] Y. Meng, B. Liu, and L. Wang, "Speed control of PMSM based on an optimized ADRC controller," *Mathematical Problems in Engineering*, vol. 2019, Article ID 1074702, 18 pages, 2019.

[8] P. Pei, Z. Pei, Z. Tang, and H. Gu, "Position tracking control of PMSM based on fuzzy PID-variable structure adaptive control," *Mathematical Problems in Engineering*, vol. 2018, Article ID 5794067, 15 pages, 2018.

[9] M. Zhang, F. Xiao, R. Shao, and Z. Deng, "Robust fault detection for permanent-magnet synchronous motor via adaptive sliding-mode observer," *Mathematical Problems in Engineering*, vol. 2020, Article ID 9360939, 6 pages, 2020.

[10] Y. Zou, Y. Hu, and S. Cao, "Model predictive control of electric spring for voltage regulation and harmonics suppression," *Mathematical Problems in Engineering*, vol. 2019, Article ID 7973591, 8 pages, 2019.

[11] H.-S. Kim, Y. Lee, S.-K. Sul, J. Yu, and J. Oh, "Online MTPA control of IPMSM based on robust numerical optimization technique," *IEEE Transactions on Industry Applications*, vol. 55, no. 4, pp. 3736–3746, 2019.

[12] J. S. Lee and R. D. Lorenz, "Robustness analysis of deadbeat-direct torque and flux control for IPMSM drives," *IEEE Transactions on Industrial Electronics*, vol. 63, no. 5, pp. 2775–2784, 2016.

[13] M. Fadel, L. Sepulchre, and M. Pietrzak-David, "Deep flux-weakening strategy with MTPV for high-speed IPMSM for vehicle application," *IFAC-PapersOnLine*, vol. 51, no. 28, pp. 616–621, 2018.

[14] W. Lin, D. Liu, Q. Wu, Q. Lu, L. Cui, and J. Wang, "Comparative study on direct torque control of interior permanent magnet synchronous motor for electric vehicle," *IFAC-PapersOnLine*, vol. 48, no. 11, pp. 65–71, 2015.

[15] H. T. Nguyen and J.-W. Jung, "Finite control set model predictive control to guarantee stability and robustness for surface-mounted pm synchronous motors," *IEEE Transactions on Industrial Electronics*, vol. 65, no. 11, pp. 8510–8519, 2018.

[16] Q. Li, L. Liu, and X. Yuan, "Model predictive controller-based optimal slip ratio control system for distributed driver electric vehicle," *Mathematical Problems in Engineering*, vol. 2020, Article ID 8086590, 15 pages, 2020.

[17] V. Q. Binh Ngo, P. R. Ayerb, S. Olaru, and S.-I. Niculescu, "Model predictive direct power control of doubly fed induction generator with dead-time compensation," *IFAC-Papers OnLine*, vol. 50, no. 1, pp. 8752–8757, 2017.

[18] A. Mbarek and K. Bouzrara, "Fault tolerant control for MIMO nonlinear systems via MPC based on MIMO ARX-laguerre multiple models," *Mathematical Problems in Engineering*, vol. 2019, Article ID 9012182, 26 pages, 2019.

[19] V.-Q.-B. Ngo, M.-K. Nguyen, T.-T. Tran, J.-H. Choi, and Y.-C. Lim, "A modified model predictive power control for grid-connected t-type inverter with reduced computational complexity," *Electronics*, vol. 8, no. 2, p. 217, 2019.

[20] J. Oravec, M. Kvasnica, and M. Bakosova, "Quasi-non-symmetric input and output constraints in LMI-based robust MPC," *IFAC-Papers OnLine*, vol. 50, no. 1, pp. 11337–11342, 2017.

[21] P. Ojaghi, N. Bigdeli, and M. Rahmani, "An LMI approach to robust model predictive control of nonlinear systems with state-dependent uncertainties," *Journal of Process Control*, vol. 47, pp. 1–10, 2016.

[22] I. Nodozi and M. Rahmani, "LMI-based robust mixed-integer model predictive control for hybrid systems," *International Journal of Control*, pp. 1–10, 2019.

[23] H. Li, S. Chen, X. Wu, and G. Tan, "Model predictive control method with constant switching frequency to reduce common-mode voltage for PMSM drives," *Journal of Electrical and Computer Engineering*, vol. 2018, Article ID 1090452, 12 pages, 2018.

[24] K. Lu, Y. Zhu, Z. Wu, and M. Xiao, "Suppression model predictive control method with constant switching frequency to reduce common-mode voltage for PMSM drives of current fluctuations and the brake torque for PMSM shutoff in electric vehicles," *Mathematical Problems in Engineering*, vol. 2019, Article ID 5026316, 13 pages, 2019.

[25] E. Can and H. H. Sayan, "Different mathematical model for the chopper circuit," *Tehnički Glasnik*, vol. 10, no. 1-2, pp. 13–15, 2016.

[26] X. Ge, M. Chen, M. Shi et al., "A single-stage buck-boost three-level neutral-point-clamped inverter with two input sources for the grid-tied photovoltaic power generation," *Mathematical Problems in Engineering*, vol. 2019, Article ID 3238159, 15 pages, 2019.

[27] S. S. Lee, C. S. Lim, Y. P. Siwakoti, and K. Lee, "Dual-t-type five-level cascaded multilevel inverter with double voltage boosting gain," *IEEE Transactions on Power Electronics*, vol. 35, no. 9, pp. 9524–9531, 2020.

[28] A. Katkout, T. Nasser, and A. Essadki, "An efficient model predictive current control algorithm for grid-connected multi-level inverter with computational delay compensation," in *Proceedings of the 2020 International Conference on Electrical and Information Technologies (ICEIT)*, pp. 1–6, Rabat, Morocco, March 2020.

[29] E. Can, "Mathematical algorithm of fuzzy logic controller for multilevel inverter creating vertical divided voltage," *Acta Polytechnica*, vol. 59, no. 1, pp. 1–11, 2019.

[30] Y. Yang, H. Wen, M. Fan et al., "Multiple-voltage-vector model predictive control with reduced complexity for multilevel inverters," *IEEE Transactions on Transportation Electrification*, vol. 6, no. 1, pp. 105–117, 2020.

[31] E. Can, "The levels effect of the voltage generated by an inverter with partial source on distortion," *International Journal of Electronics*, pp. 1–22, 2020.

[32] Y. Yu, L. Gao, Y. Liu, F. Chai, and S. Cheng, "A novel SHMPWM technique for sensorless control in high-power PMSM," *Mathematical Problems in Engineering*, vol. 2015, Article ID 315898, 9 pages, 2015.

[33] V.-Q.-B. Ngo, V.-H. Vu, V.-T. Pham et al., "Lyapunov-induced model predictive power control for grid-tie three-level neutral-point-clamped inverter with dead-time compensation," *IEEE Access*, vol. 7, pp. 166869–166882, 2019.

[34] E. Can, "The design and experimentation of the new cascaded dc-dc boost converter for renewable energy," *International Journal of Electronics*, vol. 106, no. 9, pp. 1374–1393, 2019.

[35] X. Zhang, G. Foo, and N. Tung, "Predictive torque control of three-level sparse neutral point clamped inverter fed IPMSM drives using simplified deadbeat principle," *IOP Conference Series: Earth and Environmental Science*, vol. 322, Article ID 012005, 2019.

[36] K. S. Alam, M. P. Akter, D. Xiao, D. Zhang, and M. F. Rahman, "Asymptotically stable predictive control of grid-connected converter based on discrete space vector modulation," *IEEE Transactions on Industrial Informatics*, vol. 15, no. 5, pp. 2775–2785, 2018.

[37] A. Tiga, C. Ghorbel, and N. Benhadj Braiek, "Nonlinear/linear switched control of inverted pendulum system: stability analysis and real-time implementation," *Mathematical Problems in Engineering*, vol. 2019, Article ID 2391587, 10 pages, 2019.

[38] M. Preindl, "Robust control invariant sets and lyapunov-based MPC for IPM synchronous motor drives," *IEEE Transactions on Industrial Electronics*, vol. 63, no. 6, pp. 3925–3933, 2016.

[39] T. Bariša, S. Ileš, D. Sumina, and J. Matuško, "Model predictive direct current control of a permanent magnet synchronous generator based on flexible lyapunov function considering converter dead time," *IEEE Transactions on Industry Applications*, vol. 54, no. 3, pp. 2899–2912, 2018.

[40] A. Katkout, A. Essadki, and T. Nasser, "A modified multi-objective finite control set model predictive control for three-level neutral-point clamped inverter," in *Proceedings of the 2019 International Conference on Wireless Technologies, Embedded and Intelligent Systems (WITS)*, pp. 1–6, Fez, Morocco, April 2019.

[41] J. Rodriguez and P. Cortes, Predictive Control of Power Converters and Electrical Drives, vol. 40, John Wiley & Sons, Hoboken, NJ, USA, 2012.

[42] G. Cimini, D. Bernardini, S. Levijoki, and A. Bemporad, "Embedded model predictive control with certified real-time optimization for synchronous motors," *IEEE Transactions on Control Systems Technology*, pp. 1–8, 2020.

[43] X. Zhang, G. H. B. Foo, T. Jiao, T. Ngo, and C. H. T. Lee, "A simplified deadbeat based predictive torque control for three-level simplified neutral point clamped inverter fed IPMSM drives using SVM," *IEEE Transactions on Energy Conversion*, vol. 34, no. 4, pp. 1906–1916, 2019.

[44] A. Lange and B. Piepenbreier, "Space vector modulation for three-level simplified neutral point clamped (3l-SNPC) inverter," in *Proceedings of the 2017 IEEE 18th Workshop on Control and Modeling for Power Electronics (COMPEL)*, pp. 1–8, IEEE, Stanford, CA, USA, July 2017.

[45] G. H. B. Foo, T. Ngo, X. Zhang, and M. F. Rahman, "SVM direct torque and flux control of three-level simplified neutral point clamped inverter fed interior pm synchronous motor drives," *IEEE/ASME Transactions on Mechatronics*, vol. 24, no. 3, pp. 1376–1385, 2019.

[46] H. T. Ngo, *Direct torque control strategies for interior permanent magnet synchronous motors driven by a three-level simplified neutral point clamped inverter*, Ph.D. thesis, Auckland University of Technology, Auckland, New Zealand, 2018.

[47] A. Choudhury, P. Pillay, and S. S. Williamson, "Modified dc-bus voltage balancing algorithm for a three-level neutral-point-clamped PMSM inverter drive with reduced common-mode voltage," *IEEE Transactions on Industry Applications*, vol. 52, no. 1, pp. 278–292, 2015.

[48] S. Vázquez Pérez, J. Rodríguez, M. Rivera, L. García Franquelo, and M. Norambuena, "Model predictive control for power converters and drives: advances and trends," *IEEE Transactions on Industrial Electronics*, vol. 64, no. 2, pp. 935–947, 2016.

[49] A. Katkout, A. Essadki, and T. Nasser, "An improved multi-objective finite control set model predictive control for grid connected three-level neutral-point clamped inverter," in *Proceedings of the 2019 International Conference on Advanced Communication Technologies and Networking (CommNet)*, pp. 1–6, Rabat, Morocco, April 2019.

[50] T. Bariša, S. Ileš, D. Sumina, and J. Matuško, "Flexible lyapunov function based model predictive direct current control of permanent magnet synchronous generator," in *Proceedings of the 2016 IEEE International Power Electronics and Motion Control Conference (PEMC)*, pp. 98–103, Varna, Bulgaria, September 2016.